Signal Processing 108 (2015) 421–429

Contents lists available at ScienceDirect

Signal Processing

journal homepage: www.elsevier.com/locate/sigpro

Parametric Rao test for multichannel adaptive detection of range-spread target in partially homogeneous environments

Bo Shi, Chengpeng Hao *, Chaohuan Hou, Xiaochuan Ma, Chengyan Peng

State Key Laboratory of Acoustics, Institute of Acoustics, Chinese Academy of Sciences, Beijing 100190, China

ARTICLE INFO

Article history:
Received 13 November 2013
Received in revised form
28 June 2014
Accepted 6 October 2014
Available online 15 October 2014

Keywords:
Parametric adaptive detection
Rao test
Partially homogeneous environment
Range spread target

ABSTRACT

In this paper we deal with the problem of detecting a multi-channel signal of range-spread target in the presence of Gaussian disturbance with an unknown covariance matrix. In particular, we consider the so-called partially homogeneous environment, where the disturbances in both the cells under test (primary data) and the training samples (secondary data) share the same covariance matrix up to an unknown power scaling factor. To this end, we first model the disturbance as a multichannel autoregressive (AR) process, and then develop an adaptive detector resorting to the Rao test. Remarkably, the proposed detector attains asymptotically a constant false alarm rate (CFAR) independent of the disturbance covariance matrix as well as the power scaling factor. The performance assessment conducted by Monte Carlo simulation highlights that the new receiver significantly outperforms their traditional covariance matrix-based counterparts both in AR and non-AR modeled disturbance backgrounds. Meanwhile, it requires less secondary data and is computationally more efficient.

1. Introduction

Multichannel adaptive detection of point-like targets embedded in Gaussian disturbance is an issue that has gained increasing attention among radar engineers during the last few decades. For this problem a uniformly most powerful (UMP) test does not exist due to the fact that the Neyman–Pearson likelihood ratio detector requires perfect knowledge of the disturbance covariance matrix as well as the target amplitude and phase. As a result a variety of different solutions have been explored in open literature under various settings. In particular, resorting to the generalized likelihood ratio test (GLRT), Kelly derived a constant false alarm rate (CFAR) test for detecting signals known up to a scaling factor [1], and Robey, et al. derived another CFAR test called the adaptive matched filter (AMF), based upon the so-called two-step GLRT-based design procedure [2]. Other recent solutions can be found in [3–8] and references therein. More recently, in [9–17] the aforementioned design criteria have been applied to distributed targets buried in Gaussian disturbance with an unknown covariance matrix. It naturally arises when considering detection with high-resolution radars capable of resolving a target into a number of scattering centres appearing in different range cells [18].

However, all above detectors usually involve estimating and inverting a large-size space–time covariance matrix of the disturbance signal using target-free secondary data. As a consequence, they require a large number of secondary signals and excessive computation power, especially when the joint space–time dimension is large. A possible means to reduce the computational and secondary requirement is to model the disturbance as a multichannel autoregressive (AR) process, considering the fact that the multichannel AR process is not only effective to model real-world airborne radar clutter for STAP detection [19], but also versatile in capturing the temporal and the spatial correlation of

* Corresponding author at: Institute of Acoustics, Chinese Academy of Sciences, Beijing 100190, China. Fax: +86 010 8254 7706.
E-mail addresses: tthrx@126.com (B. Shi), haochengp@mail.ioa.ac.cn (C. Hao).

http://dx.doi.org/10.1016/j.sigpro.2014.10.007
0165-1684/

disturbance signals in radar and array processing applications [20,21]. The classic parametric adaptive detectors include the parametric AMF (P-AMF) [19,22], parametric Rao test (P-RAO) [23], and parametric GLRT (P-GLRT) [24,25]. Moreover, in [26], the P-RAO is generalized to address the problem of detecting a multi-channel signal of range-spread targets. It should be noted that these solutions assume a homogeneous environment, wherein the secondary data, which are free of signal, share the same covariance matrix of the disturbance in the sample under test (primary data).

More recently, in [27], adaptive parametric detection of point-like targets in partially homogeneous environment has been addressed, where two parametric Rao tests, known as the Normalized Parametric Rao Test (NP-RAO) and the Scale-Invariant Parametric Rao Test (SI-PRAO), have been devised. The partially homogeneous environment is a scenario where the primary data share the same covariance matrix with the secondary data up to an unknown power scaling factor under the null hypothesis. This scenario is motivated by the following observation that the under testing cells and the secondary range cells are separated by a band of guarding cells, and this may lead to a power difference between the testing and training signals, especially when primary cells are range spread. Detection of distributed targets in partially homogeneous environment, based upon the GLRT, has been addressed in [9]. Moreover, in [28] the same problem is attacked, where two adaptive detectors are devised relying on the Rao test and the Wald test design criteria as alternatives to the GLRT. To the best of our knowledge, however, the problem of adaptive parametric detection of distributed targets in partially homogeneous environment has not been considered, which is another motivation of this work.

In this paper we focus on the design of adaptive radar detector for distributed targets by modelling the disturbance as a multi-channel AR process in partially homogeneous environment. To this end, we apply the Rao test design criterion, which is easier to derive and implement than the GLRT, and is also asymptotically equivalent to the latter. The proposed Rao test is referred to as the generalized scale-invariant parametric Rao (GSI-PRAO). The asymptotical distribution of the proposed detector is derived in the closed form. It is shown that the GSI-PRAO is asymptotically independent of the unknown parameters in the null hypothesis, which results in the property of CFAR. The performance assessment, conducted by Monte Carlo simulation, shows the superiority of the GSI-PRAO with respect to traditional covariance matrix-based counterparts, such as the GLRT and GASD detectors [9].

The remainder of the paper is organized as follows. Section 2 contains problem formulation while Section 3 is devoted to detector designs. Section 4 contains some illustrative examples. Finally, concluding remarks and hints for future research are given in Section 5.

2. Problem formulation

We begin with the problem of detecting a known J channel signal of unknown amplitude in a spatially and temporally colored disturbance. Moreover the target is contained in H range cells enclosed with K secondary range cells where no target is supposed in. The detection problem at hand can be formulated as the following binary hypothesis test:

$$\begin{cases} H_0: \boldsymbol{r}_h = \boldsymbol{d}_h; \\ H_1: \boldsymbol{r}_h = \alpha_h \boldsymbol{a} + \boldsymbol{d}_h. \end{cases} \quad h = 1, 2, \ldots, H \tag{1}$$

with

- $\boldsymbol{r}_h = [\boldsymbol{r}_h^T(0), \boldsymbol{r}_h^T(1), \ldots, \boldsymbol{r}_h^T(N-1)]^T \in \mathbb{C}^{JN\times 1}$ denotes the testing signal;
- $\boldsymbol{a} = [\boldsymbol{a}^T(0), \boldsymbol{a}^T(1), \ldots, \boldsymbol{a}^T(N-1)]^T \in \mathbb{C}^{JN\times 1}$ denotes the nominal space–time steering vector;
- $\boldsymbol{d}_h = [\boldsymbol{d}_h^T(0), \boldsymbol{d}_h^T(1), \ldots, \boldsymbol{d}_h^T(N-1)]^T \in \mathbb{C}^{JN\times 1}$ denotes the mutually independent and identical distributed complex Gaussian random vector accounting for jammer, clutter and thermal noise;

and α_h denotes the unknown deterministic reflection factor accounting for both target reflectivity and channel effects. Usually only observing the testing signal is not sufficient for an effective estimation and detection. So it is practical to obtain the secondary data from the range cells adjacent to the primary ones, and the secondary data can be described as

$$\boldsymbol{r}_k = \boldsymbol{d}_k, \quad k = 1, 2, \ldots, K \tag{2}$$

Note that in some cases the secondary range cells may be limited or even unavailable. So it is necessary to consider the situation when K is small.

In the partially homogeneous environment, the distribution of the disturbance signals $\{\boldsymbol{d}_h\}_{h=1}^{H}$ and $\{\boldsymbol{d}_k\}_{k=1}^{K}$ can be described as a zero mean complex Gaussian random process with covariance $\boldsymbol{R}$ and $\lambda\boldsymbol{R}$, namely $\boldsymbol{d}_h \sim CN(\boldsymbol{0}, \boldsymbol{R})$ and $\boldsymbol{d}_k \sim CN(\boldsymbol{0}, \lambda\boldsymbol{R})$, respectively. As mentioned earlier λ is the unknown power scaling factor. If $\lambda = 1$, the partially homogeneous environment reduces to the homogeneous case. To model the disturbance as a J-channel AR(P) process with order P, we follow the assumption adopted by most model based detectors, see [19,30] and reference therein for proofs and analysis

$$\boldsymbol{d}_i(n) = -\sum_{p=1}^{P} \boldsymbol{A}^H(p)\boldsymbol{d}_i(n-p) + \epsilon_i(n) \tag{3}$$

where $\{\boldsymbol{A}(p)\}_{p=1}^{P}$ are the unknown $J\times J$ AR coefficient matrices, $\epsilon_i(n)$ are the driving J-channel spatial noise vectors, which are temporally white but spatially colored Gaussian noise, namely $\epsilon_i \sim CN(\boldsymbol{0}, \boldsymbol{Q}) i = 1, \ldots, H$, and $\epsilon_i \sim CN(\boldsymbol{0}, \lambda\boldsymbol{Q}) i = 1+H, \ldots, H+K$, where $\boldsymbol{Q}$ denotes the unknown $J\times J$ spacial covariance matrix, λ is the same as the one scaling the time–space covariance matrix $\boldsymbol{R}$. Note that the AR coefficient matrices are identical across all range cells, but the scaling factor differs from the secondary data, hence the environment is partially homogeneous only with respect to the spatial domain. This is reasonable since the testing and secondary data are all obtained during the same coherent pulses interval and the disturbance is supposed to be wide sense stationary.

3. Parametric Rao test

The problem of interest is to develop a parametric test based on the unknown nuisance parameters $\boldsymbol{A}(p), \boldsymbol{Q}, \lambda$ and α_h. Since there is no closed form solution [26] of a GLRT for the above range-spread target detection, we turn to the Rao test which is asymptotically the same as GLRT. The Rao test [29] for the problem of interest follows as

$$\frac{\partial \ln f(\boldsymbol{r}|\boldsymbol{\theta})}{\partial \boldsymbol{\theta}_r}\Big|_{\theta=\hat{\boldsymbol{\theta}}_0}^{T} [\boldsymbol{J}^{-1}(\hat{\boldsymbol{\theta}}_0)]_{\boldsymbol{\theta}_r,\boldsymbol{\theta}_r} \frac{\partial \ln f(\boldsymbol{r}|\boldsymbol{\theta})}{\partial \boldsymbol{\theta}_r}\Big|_{\theta=\hat{\boldsymbol{\theta}}_0} \tag{4}$$

where

- $\boldsymbol{\theta}=[\boldsymbol{\theta}_r^T,\boldsymbol{\theta}_s^T]^T$ contains all unknown parameters;
- $\hat{\boldsymbol{\theta}}_0$ is the maximum likelihood (ML) estimation of $\boldsymbol{\theta}$ under H_0 hypothesis;
- $\boldsymbol{\theta}_r=[\boldsymbol{\alpha}_R^T,\boldsymbol{\alpha}_I^T]\in\mathbb{R}^{2H\times 1}$ is the primary parameter;
- $\boldsymbol{\theta}_s=[\lambda,\boldsymbol{a}_R,\boldsymbol{a}_I,\boldsymbol{q}_R,\boldsymbol{q}_I]^T\in\mathbb{R}^{((2P+1)J^2+1)\times 1}$ is the nuisance parameter vector, with $\boldsymbol{a}_R$ and $\boldsymbol{a}_I$ being the real and the imaginary part of $vec(\boldsymbol{A}^H)$, $\boldsymbol{q}_R$ are the diagonal elements and the elements below the diagonal in $\boldsymbol{Q}$, while $\boldsymbol{q}_I$ is the imaginary part of the elements below the diagonal;
- $\boldsymbol{\alpha}_R$ and $\boldsymbol{\alpha}_I$ denote the real and the imaginary part of $\boldsymbol{\alpha}=[\alpha_1,\ldots,\alpha_H]^T$;
- $\boldsymbol{J}^{-1}(\hat{\boldsymbol{\theta}}_0)$ is the inverse of the Fisher information matrix (FIM) at the ML estimate of $\boldsymbol{\theta}$ under H_0, and the FIM can be further partitioned as

$$\boldsymbol{J}(\boldsymbol{\theta})=\begin{bmatrix}\boldsymbol{J}_{\boldsymbol{\theta}_r,\boldsymbol{\theta}_r}(\boldsymbol{\theta}) & \boldsymbol{J}_{\boldsymbol{\theta}_r,\boldsymbol{\theta}_s}(\boldsymbol{\theta})\\ \boldsymbol{J}_{\boldsymbol{\theta}_s,\boldsymbol{\theta}_r}(\boldsymbol{\theta}) & \boldsymbol{J}_{\boldsymbol{\theta}_s,\boldsymbol{\theta}_s}(\boldsymbol{\theta})\end{bmatrix} \tag{5}$$

To derive the Rao test we need to get the ML estimation of the parameters under H_0 at first. The joint probability function (pdf) of the receiving data $f(\boldsymbol{r}|\boldsymbol{\theta})$, conditioned on the first P elements, can be expressed as (see Appendix A for derivation)

$$f(\boldsymbol{r}|\boldsymbol{\theta})=\left[\frac{\lambda^{-JK/(K+H)}}{\pi^{J}|\boldsymbol{Q}|}\exp\{-\mathrm{tr}(\boldsymbol{Q}^{-1}\boldsymbol{T}(\boldsymbol{\theta}))\}\right]^{(H+K)(N-P)}, \tag{6}$$

where $\mathrm{tr}(\cdot)$ denotes the matrix trace operator, and

$$(H+K)(N-P)\boldsymbol{T}(\boldsymbol{\theta})=\sum_{h=1}^{H}\sum_{n=P}^{N-1}\boldsymbol{\epsilon}_h(n)\boldsymbol{\epsilon}_h^H(n)+\frac{1}{\lambda}\sum_{k=1}^{K}\sum_{n=P}^{N-1}\boldsymbol{\epsilon}_k(n)\boldsymbol{\epsilon}_k^H(n). \tag{7}$$

In (7), $\boldsymbol{\epsilon}_h(n)$, $h=1,\ldots,H$ are the temporally whitened testing signals

$$\begin{aligned}\boldsymbol{\epsilon}_h(n)&=\tilde{\boldsymbol{r}}_h(n)-\alpha_h\tilde{\boldsymbol{a}}(n)\\&=\left[\boldsymbol{r}_h(n)+\sum_{p=1}^{P}\boldsymbol{A}^H(p)\boldsymbol{r}_h(n-p)\right]\\&\quad-\alpha_h\left[\boldsymbol{a}(n)+\sum_{p=1}^{P}\boldsymbol{A}^H(p)\boldsymbol{a}(n-p)\right],\end{aligned} \tag{8}$$

and $\boldsymbol{\epsilon}_k(n)$, $k=1,\ldots,K$ denote the temporally whitened training signals

$$\boldsymbol{\epsilon}_k(n)=\boldsymbol{r}_k(n)+\sum_{p=1}^{P}\boldsymbol{A}^H(p)\boldsymbol{r}_k(n-p). \tag{9}$$

Note that $\boldsymbol{\alpha}=\boldsymbol{0}$ results in the pdf under H_0, and take the derivative of log-likelihood function $\ln f(\boldsymbol{r}|\boldsymbol{\theta})|_{\boldsymbol{\alpha}=\boldsymbol{0}}$, with respect to (w.r.t.) $\boldsymbol{Q}$, and equate it to zero, we can get the estimation of $\boldsymbol{Q}$

$$\hat{\boldsymbol{Q}}(\lambda,\boldsymbol{A})=\frac{1}{(H+K)(N-P)}\sum_{h=1}^{H}\sum_{n=P}^{N-1}\boldsymbol{\epsilon}_h(n)\boldsymbol{\epsilon}_h^H(n)+\frac{1}{\lambda}\sum_{k=1}^{K}\sum_{n=P}^{N-1}\boldsymbol{\epsilon}_k(n)\boldsymbol{\epsilon}_k^H(n). \tag{10}$$

Note that $\boldsymbol{T}(\lambda,\boldsymbol{A})|_{\boldsymbol{\alpha}=\boldsymbol{0}}$ is the ML estimation of $\hat{\boldsymbol{Q}}$, and $\boldsymbol{T}(\lambda,\boldsymbol{A})|_{\boldsymbol{\alpha}=\boldsymbol{0}}$ can be rewritten as

$$(H+K)(N-P)\boldsymbol{T}(\lambda,\boldsymbol{A})|_{\boldsymbol{\alpha}=\boldsymbol{0}}=\hat{\boldsymbol{R}}_{rr}(\lambda)+\boldsymbol{A}^H\hat{\boldsymbol{R}}_{tr}(\lambda)+\hat{\boldsymbol{R}}_{tr}^H(\lambda)\boldsymbol{A}+\boldsymbol{A}^H\hat{\boldsymbol{R}}_{tt}^H(\lambda)\boldsymbol{A} \tag{11}$$

where $\boldsymbol{A}^H=[\boldsymbol{A}^H(1),\ldots,\boldsymbol{A}^H(P)]$, and the correlation matrices are defined as

$$\hat{\boldsymbol{R}}_{rr}(\lambda)=\sum_{n=P}^{N-1}\left[\sum_{h=1}^{H}\boldsymbol{r}_h(n)\boldsymbol{r}_h^H(n)+\frac{1}{\lambda}\sum_{k=1}^{K}\boldsymbol{r}_k(n)\boldsymbol{r}_k^H(n)\right] \tag{12}$$

$$\hat{\boldsymbol{R}}_{tr}(\lambda)=\sum_{n=P}^{N-1}\left[\sum_{h=1}^{H}\boldsymbol{t}_h(n)\boldsymbol{r}_h^H(n)+\frac{1}{\lambda}\sum_{k=1}^{K}\boldsymbol{t}_k(n)\boldsymbol{r}_k^H(n)\right] \tag{13}$$

$$\hat{\boldsymbol{R}}_{tt}(\lambda)=\sum_{n=P}^{N-1}\left[\sum_{h=1}^{H}\boldsymbol{t}_h(n)\boldsymbol{t}_h^H(n)+\frac{1}{\lambda}\sum_{k=1}^{K}\boldsymbol{t}_k(n)\boldsymbol{t}_k^H(n)\right] \tag{14}$$

with $\boldsymbol{t}_i=[\boldsymbol{r}_i^T(n-1),\ldots,\boldsymbol{r}_i^T(n-P)]^T\in\mathbb{C}^{JP\times 1}$, $i=h$ or k. Taking the derivative of (11) w.r.t. $\boldsymbol{A}$ and equating it to zero, we get the ML estimation of $\boldsymbol{A}^H$, which is

$$\hat{\boldsymbol{A}}_{\lambda}^{H}=-\hat{\boldsymbol{R}}_{tr}^{H}(\lambda)\hat{\boldsymbol{R}}_{tt}^{-1}(\lambda) \tag{15}$$

put (15) into (11) we have

$$\hat{\boldsymbol{Q}}_{ML}=\frac{\hat{\boldsymbol{R}}_{rr}(\hat{\lambda})+\hat{\boldsymbol{A}}_{\hat{\lambda}}^{H}\hat{\boldsymbol{R}}_{tr}(\hat{\lambda})}{(H+K)(N-P)} \tag{16}$$

where $\hat{\lambda}$ is the solution of the following equation (see Appendix B for details):

$$\frac{JK}{H+K}-\sum_{i=1}^{J(P+1)}\frac{1}{1+\lambda\tau_i}+\sum_{i=1}^{JP}\frac{1}{1+\lambda\gamma_i}=0 \tag{17}$$

where $\{\tau_i\}_{i=1}^{J(P+1)}$ and $\{\gamma_i\}_{i=1}^{JP}$ are the eigenvalues of the matrices $\hat{\boldsymbol{R}}_K^{-1/2}\hat{\boldsymbol{R}}_H\hat{\boldsymbol{R}}_K^{-1/2}$ and $\hat{\boldsymbol{R}}_{K,t}^{-1/2}\hat{\boldsymbol{R}}_{H,t}\hat{\boldsymbol{R}}_{K,t}^{-1/2}$, respectively, with

$$\hat{\boldsymbol{R}}_H=\begin{bmatrix}\sum_{h=1}^{H}\sum_{n=P}^{N-1}\boldsymbol{t}_h(n)\boldsymbol{t}_h^H(n) & \sum_{h=1}^{H}\sum_{n=P}^{N-1}\boldsymbol{t}_h(n)\boldsymbol{r}_h^H(n)\\ \sum_{h=1}^{H}\sum_{n=P}^{N-1}\boldsymbol{r}_h(n)\boldsymbol{t}_h^H(n) & \sum_{h=1}^{H}\sum_{n=P}^{N-1}\boldsymbol{r}_h(n)\boldsymbol{r}_h^H(n)\end{bmatrix} \tag{18}$$

$$\hat{\boldsymbol{R}}_K=\begin{bmatrix}\sum_{k=1}^{K}\sum_{n=P}^{N-1}\boldsymbol{t}_k(n)\boldsymbol{t}_k^H(n) & \sum_{k=1}^{K}\sum_{n=P}^{N-1}\boldsymbol{t}_k(n)\boldsymbol{r}_k^H(n)\\ \sum_{k=1}^{K}\sum_{n=P}^{N-1}\boldsymbol{r}_k(n)\boldsymbol{t}_k^H(n) & \sum_{k=1}^{K}\sum_{n=P}^{N-1}\boldsymbol{r}_k(n)\boldsymbol{r}_k^H(n)\end{bmatrix} \tag{19}$$

$$\hat{\boldsymbol{R}}_{H,t}=\sum_{h=1}^{H}\sum_{n=P}^{N-1}\boldsymbol{t}_h(n)\boldsymbol{t}_h^H(n) \tag{20}$$

$$\hat{\boldsymbol{R}}_{K,t}=\sum_{k=1}^{K}\sum_{n=P}^{N-1}\boldsymbol{t}_k(n)\boldsymbol{t}_k^H(n) \tag{21}$$

3.1. FIM and first-order derivatives of the log likelihood function

In this subsection, the FIM and formulas related to it are derived. Note that the vectors $\boldsymbol{\theta}_r$ and $\boldsymbol{\theta}_s$ have no parameter in common. This result in $\boldsymbol{J}_{\boldsymbol{\theta}_s,\boldsymbol{\theta}_r}(\boldsymbol{\theta})=\mathbf{0}$ and $\boldsymbol{J}_{\boldsymbol{\theta}_r,\boldsymbol{\theta}_s}(\boldsymbol{\theta})=\mathbf{0}$. So we have

$$[\boldsymbol{J}^{-1}(\boldsymbol{\theta})]_{\boldsymbol{\theta}_r,\boldsymbol{\theta}_r}=\boldsymbol{J}^{-1}_{\boldsymbol{\theta}_r,\boldsymbol{\theta}_r}(\boldsymbol{\theta}) \tag{22}$$

The hth element of the first-order partial derivative of the log likelihood function of $f(\boldsymbol{r}|\boldsymbol{\theta})$ w.r.t $\boldsymbol{\theta}_r$ is

$$\left[\frac{\partial \ln f(\boldsymbol{r}|\boldsymbol{\theta})}{\partial \boldsymbol{\theta}_r}\right]_h=\left[\begin{array}{c}\dfrac{\partial \ln f(\boldsymbol{r}|\boldsymbol{\theta})}{\partial \boldsymbol{\alpha}_R}\\ \dfrac{\partial \ln f(\boldsymbol{r}|\boldsymbol{\theta})}{\partial \boldsymbol{\alpha}_I}\end{array}\right]_h \tag{23}$$

in particular

$$\left[\frac{\partial \ln f(\boldsymbol{r}|\boldsymbol{\theta})}{\partial \boldsymbol{\alpha}_R}\right]_h=\sum_{n=P}^{N-1}\mathrm{Re}\left[\tilde{\boldsymbol{a}}^H(n)\boldsymbol{Q}^{-1}\tilde{\boldsymbol{r}}_h(n)\right] \tag{24}$$

$$\left[\frac{\partial \ln f(\boldsymbol{r}|\boldsymbol{\theta})}{\partial \boldsymbol{\alpha}_I}\right]_h=\sum_{n=P}^{N-1}\mathrm{Im}\left[\tilde{\boldsymbol{a}}^H(n)\boldsymbol{Q}^{-1}\tilde{\boldsymbol{r}}_h(n)\right] \tag{25}$$

where $[\cdot]_h$ denotes the hth element of a vector, the temporal whitened steering vector $\tilde{\boldsymbol{a}}(n)$ and the temporal whitened testing signal $\tilde{\boldsymbol{r}}_h(n)$ can be obtained by replacing the AR coefficient in (8) with its ML estimation. The second-order partial derivatives are

$$\frac{\partial^2 \ln f(\boldsymbol{r}|\boldsymbol{\theta})}{\partial\{\boldsymbol{\alpha}_R\}_i\partial\{\boldsymbol{\alpha}_R\}_h}=-\delta(i-h)2\sum_{n=P}^{N-1}\tilde{\boldsymbol{a}}^H(n)\boldsymbol{Q}^{-1}\tilde{\boldsymbol{a}}(n) \tag{26}$$

$$\frac{\partial^2 \ln f(\boldsymbol{r}|\boldsymbol{\theta})}{\partial\{\boldsymbol{\alpha}_I\}_i\partial\{\boldsymbol{\alpha}_I\}_h}=-\delta(i-h)2\sum_{n=P}^{N-1}\tilde{\boldsymbol{a}}^H(n)\boldsymbol{Q}^{-1}\tilde{\boldsymbol{a}}(n) \tag{27}$$

$$\frac{\partial^2 \ln f(\boldsymbol{r}|\boldsymbol{\theta})}{\partial\{\boldsymbol{\alpha}_R\}_i\partial\{\boldsymbol{\alpha}_I\}_h}=\frac{\partial^2 \ln f(\boldsymbol{r}|\boldsymbol{\theta})}{\partial\{\boldsymbol{\alpha}_I\}_i\partial\{\boldsymbol{\alpha}_R\}_h}=0 \tag{28}$$

where $\delta(l)$ is the Kronecker delta function. Plugging (26)–(28) into (22) results in

$$[\boldsymbol{J}^{-1}(\boldsymbol{\theta}_0)]_{\boldsymbol{\theta}_r,\boldsymbol{\theta}_r}=\frac{1}{2\sum_{n=P}^{N-1}\tilde{\boldsymbol{a}}^H(n)\hat{\boldsymbol{Q}}_{ML}^{-1}\tilde{\boldsymbol{a}}(n)}\boldsymbol{I}_{2H} \tag{29}$$

where $\boldsymbol{I}_{2H}$ denotes the identity matrix with $2H$ diagonal elements. Putting (24), (25) and (29) back into (4) *we get the GSI-PRAO as follows*:

$$T_{\mathrm{GSI-PRAO}}\triangleq\frac{2\sum_{h=1}^{H}|\sum_{n=P}^{N-1}\tilde{\boldsymbol{a}}^H(n)\hat{\boldsymbol{Q}}_{ML}^{-1}\tilde{\boldsymbol{r}}_h(n)|^2}{\sum_{n=P}^{N-1}\tilde{\boldsymbol{a}}^H(n)\hat{\boldsymbol{Q}}_{ML}^{-1}\tilde{\boldsymbol{a}}(n)}\underset{H_0}{\overset{H_1}{\gtrless}}\eta, \tag{30}$$

where η is a proper threshold to be set.

3.2. Asymptotic performance

According to [29], the GSI-PRAO has the same asymptotic distribution with the GLRT when $N\to\infty$. So we have

$$T_{\mathrm{GSI-PRAO}}\overset{a}{\sim}\begin{cases}\chi^2_{2H} & H_0\\ \chi'^2_{2H}(\xi) & H_1\end{cases} \tag{31}$$

where χ^2_{2H} is the central Chi-squared distribution with $2H$ degrees of freedom, and $\chi'^2_{2H}(\xi)$ is the non-central Chi-squared distribution with $2H$ degrees of freedom and a non-central parameter ξ

$$\begin{aligned}\xi&=(\boldsymbol{\theta}_r-\boldsymbol{\theta}_{0r})^T([\boldsymbol{J}^{-1}(\boldsymbol{\theta})]_{\boldsymbol{\theta}_r,\boldsymbol{\theta}_r})^{-1}(\boldsymbol{\theta}_r-\boldsymbol{\theta}_{0r})\\&=2\sum_{h=1}^{H}|\alpha_h|^2\sum_{n=P}^{N-1}\tilde{\boldsymbol{a}}^H(n)\boldsymbol{Q}^{-1}\tilde{\boldsymbol{a}}(n)\end{aligned} \tag{32}$$

where $\boldsymbol{\theta}_{0r}=\mathbf{0}\in\mathbb{R}^{2H\times 1}$ is the primary parameter under H_0 and $\tilde{\boldsymbol{a}}$ is generated by using the true AR coefficient matrix A (in Section 4 we generate the simulation data with a give AR coefficient matrix). For a given asymptotic test threshold η, the asymptotic probability of false alarm can be denoted as

$$P_{fa}=\int_{\eta}^{+\infty}f_{\chi^2_{2H}}(x)\,dx=\int_{\eta}^{+\infty}\frac{1}{2^H\Gamma(H)}x^{H-1}e^{-x/2}\,dx \tag{33}$$

where $f_{\chi^2_{2H}}(x)$ is the pdf of χ^2_{2H}, and $\Gamma(\cdot)$ is the gamma function. According to (33) the probability of false alarm is only related to H and the chosen threshold. This implies the GSI-PRAO test is asymptotically constant false alarm rate (CFAR). Furthermore, the asymptotic detection probability is expressed as

$$\begin{aligned}P_d&=\int_{\eta}^{+\infty}f_{\chi'^2_{2H}}(x)\,dx\\&=\int_{\eta}^{+\infty}\frac{1}{2}\left(\frac{x}{\xi}\right)^{(H-1)/2}\exp\left(-\frac{\xi+x}{2}\right)\boldsymbol{I}_{H-1}\left(\sqrt{\xi x}\right)dx\end{aligned} \tag{34}$$

where $f_{\chi'^2_{2H}}(x)$ is the pdf of χ'^2_{2H}, and $\boldsymbol{I}_{H-1}(\cdot)$ is the modified Bessel function of the first kind with the $(H-1)$th order.

4. Performance assessment

Before representing the simulation results, we give some necessary definitions first. The disturbance signal is generated as a second-order multichannel AR process, except for the "Model-mismatched case" subsection. The AR(2) coefficient matrices $\boldsymbol{A}$ and spatial covariance matrix $\boldsymbol{Q}$ are generated from a given space–time covariance matrix $\boldsymbol{R}\in\mathbb{C}^{JN\times JN}$ which is previously generated using the method in [31]. The space–time steering vector is given by

$$\boldsymbol{a}=\boldsymbol{a}_t(f_d)\otimes\boldsymbol{a}_s(f_s) \tag{35}$$

where $\boldsymbol{a}_t(f_d)$ is the $N\times 1$ temporal steering vector with f_d the normalized Doppler frequency

$$\boldsymbol{a}_t=\frac{1}{\sqrt{N}}[1,e^{if_d},\ldots,e^{i(N-1)f_d}]^T \tag{36}$$

and $\boldsymbol{a}_s(f_s)$ is the $J\times 1$ temporal steering vector with f_s the normalized spatial frequency

$$\boldsymbol{a}_s=\frac{1}{\sqrt{J}}[1,e^{if_s},\ldots,e^{i(N-1)f_s}]^T. \tag{37}$$

The signal to noise ratio (SNR) is defined as

$$SNR=\sum_{h=1}^{H}\frac{|\alpha_h|^2}{H}\boldsymbol{a}^H\boldsymbol{R}^{-1}\boldsymbol{a}. \tag{38}$$

In the numerical simulations two detectors which are derived in [9] to handle the similar detection problem are included. It is interesting to see if our detectors are more competitive in different cases, especially in the limited secondary data case. For easy reference, we rewrite

the two detectors below

$$T_{\mathrm{GLRT}}=\frac{\hat{\lambda}_0^{JK/(K+H)}|\boldsymbol{Z}_0+\hat{\lambda}_0^{-1}\boldsymbol{S}|}{\hat{\lambda}_1^{JK/(K+H)}|\boldsymbol{Z}_0+\hat{\lambda}_1^{-1}\boldsymbol{S}|} \tag{39}$$

where

$$\boldsymbol{Z}_0=\sum_{h=1}^{H}\boldsymbol{r}_h\boldsymbol{r}_h^H,$$

$$\boldsymbol{Z}_1=\sum_{h=1}^{H}\left(\boldsymbol{r}_h-\frac{\boldsymbol{a}^H\boldsymbol{S}^{-1}\boldsymbol{r}_h}{\boldsymbol{a}^H\boldsymbol{S}^{-1}\boldsymbol{a}}\boldsymbol{a}\right)\left(\boldsymbol{r}_h-\frac{\boldsymbol{a}^H\boldsymbol{S}^{-1}\boldsymbol{r}_h}{\boldsymbol{a}^H\boldsymbol{S}^{-1}\boldsymbol{a}}\boldsymbol{a}\right)^H \quad \text{and} \quad \boldsymbol{S}=\sum_{k=1}^{K}\boldsymbol{r}_k\boldsymbol{r}_k^H.$$

The scaling factors λ_0 and λ_1 are estimated using the following equation:

$$\sum_{i=1}^{b_j}\frac{\gamma_{i,j}\lambda_j}{\gamma_{i,j}\lambda_j+1}=\frac{JNH}{K+H},\quad j=0,1 \tag{40}$$

where $b_0=\min(H,JN)$, $\gamma_{i,0}$ denotes the nonzero eigenvalue of the matrix $\boldsymbol{S}^{-1/2}\boldsymbol{Z}_0\boldsymbol{S}^{-1/2}$ under H_0, $b_1=\min(H,JN-1)$ and $\gamma_{i,1}$ denotes the nonzero eigenvalue of the matrix $\boldsymbol{S}^{-1/2}\boldsymbol{Z}_1\boldsymbol{S}^{-1/2}$ under H_1

$$T_{\mathrm{GASD}}=\sum_{h=1}^{H}\frac{|\boldsymbol{a}^H\boldsymbol{S}^{-1}\boldsymbol{r}_h|^2}{\boldsymbol{a}^H\boldsymbol{S}^{-1}\boldsymbol{a}\sum_{i=1}^{H}\boldsymbol{r}_h^H\boldsymbol{S}^{-1}\boldsymbol{r}_h} \tag{41}$$

The following simulation results are obtained for various values of K, N, λ and multiple dominant scatterer (MDS) models when $J=4$, $P=2$, $H=8$ and a constant false alarm $P_{fa}=10^{-2}$. In particular, we make five distinct comparisons: (1) the limited secondary data case. In this case, we restrict $K=1$ (the minimum value) to ensure an effective estimation of λ, and evaluate the detection performance in different values of the number of sampling pulses; (2) the asymptotic case. We evaluate the asymptotic performance by increasing the secondary data; (3) the scaling invariant case. In this case different power scaling factors are set to evaluate the CFAR property of the GSI-PRAO in comparison with the other two detectors; (4) the model mismatched case. We evaluate the GSI-PRAO's performance when the AR-model order is not accurate or the disturbance is not an AR process; (5) the MDS models case. We utilize the different MDS models defined in Table 1 to evaluate the influence of those models. In above each case, the asymptotic curve (34) obtained by using the true AR coefficients $\boldsymbol{A}$ and $\boldsymbol{Q}$ is also included to serve as a benchmark.

4.1. Limited-training case

In this case, the simulation is carried out under Model0. Figs. 1 and 2 show the probability of detection (P_d) versus SNR for $J=4$, $N=16$, and $\lambda=4$. Moreover, for the GSI-PRAO, we set

Table 1
MDS models.

Model	Range cell							
number	1	2	3	4	5	6	7	8
Model0	1/8	1/8	1/8	1/8	1/8	1/8	1/8	1/8
Model1	1/12	1/12	1/12	5/12	1/12	1/12	1/12	1/12
model2	1	0	0	0	0	0	0	0

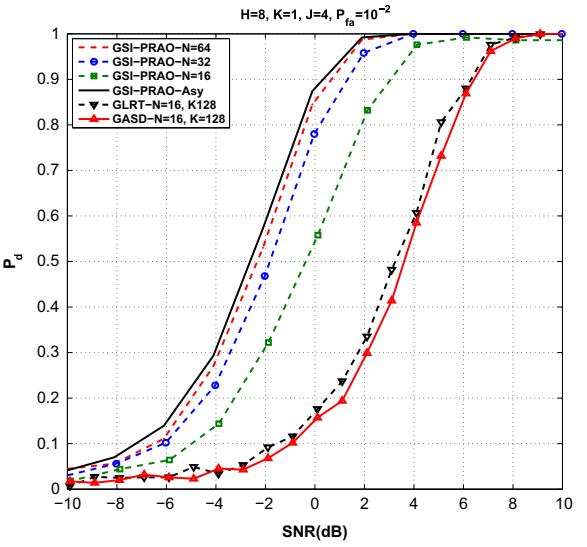

Fig. 1. Probability of detection vs. SNR for different numbers of pulses when $P_f=0.01$, $J=4$, $K=1$ and $\lambda=4$.

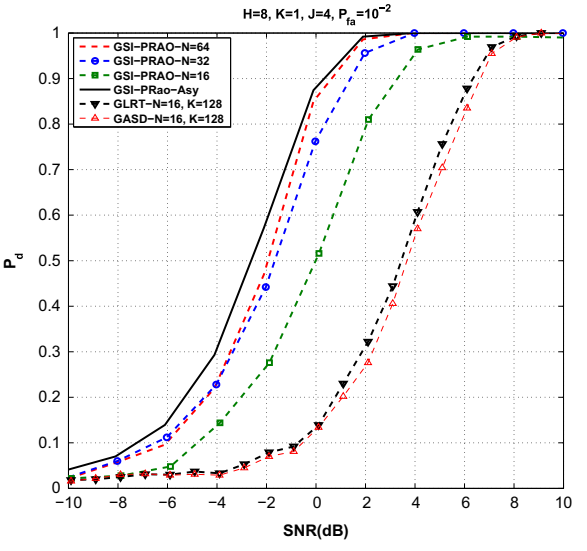

Fig. 2. Probability of detection vs. SNR for different numbers of pulses when $P_f=0.01$, $J=4$, $K=1$ and $\lambda=8$.

$K=1$, and consider two other cases of N, i.e., $N=32$ and $N=64$. For the GLRT and GASD, we set $K=128$ in order to make sure that the sample covariance matrix is non-singular.

It is clear that the GSI-PRAO performs much better than the GLRT and GASD in this limited-training case. What's more, the larger the number of sampling pulses is, the closer the simulation curves approach to the asymptotic one.

4.2. Asymptotic case and the scaling invariant property

Firstly, we evaluate the detection performance with limited sampling pulses. Figs. 3 and 4 show P_d versus SNR when $\lambda=4$ and $\lambda=8$, respectively. Both figures show that the P_d curves of the GSI-PRAO approach its asymptotic performance as K increases. This property is similar to the

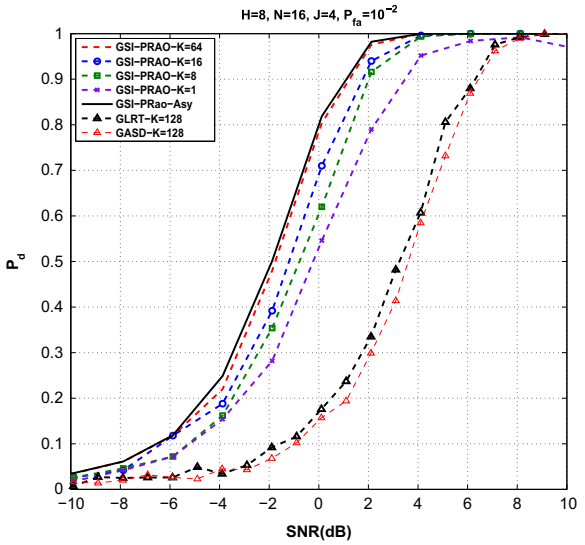

Fig. 3. Probability of detection vs. SNR for different numbers of training signals when $P_f=0.01$, $J=4$, $N=16$, $\lambda=4$.

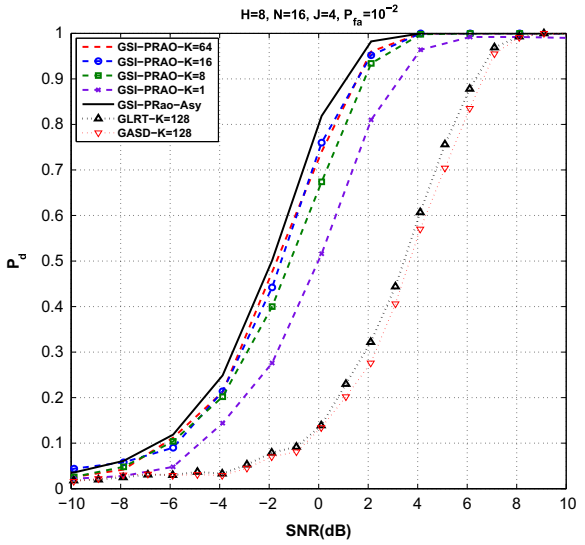

Fig. 4. Probability of detection vs. SNR for different numbers of training signals when $P_f=0.01$, $J=4$, $N=16$, and $\lambda=8$.

scenario when N increases, and implies that the parametric method overcomes the lack of secondary data by adopting more sampling pulses. Meanwhile, the GSI-PRAO with different values of K outperforms the GLRT and GASD with $K=128$.

Furthermore, in Fig. 5 we evaluate the detection performance for several values of λ. Note that when $\lambda=1$, the partially homogeneous environment turns to be a ideally homogeneous environment, where the GSI-PRAO is expected to perform no worse than the partially homogeneous environment. Indeed, the figure shows that all P_d curves of the considered three detectors converge to a potential common center. This result implies that all three detectors have the CFAR property w.r.t. λ.

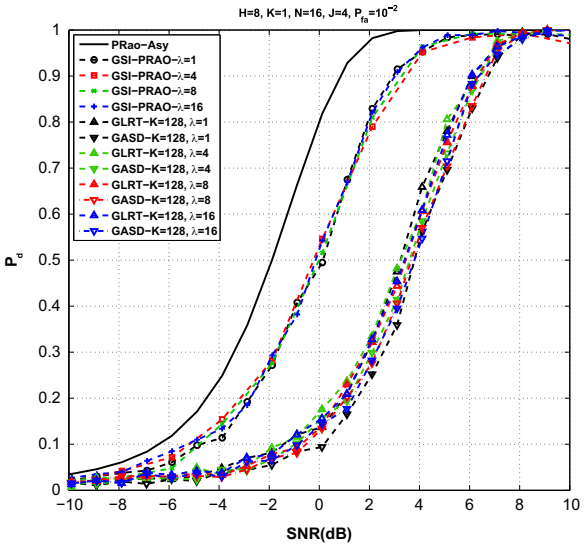

Fig. 5. Probability of detection vs. SNR for different covariance power scaling factors when $P_f=0.01$, $J=4$, $N=16$, $K=1$.

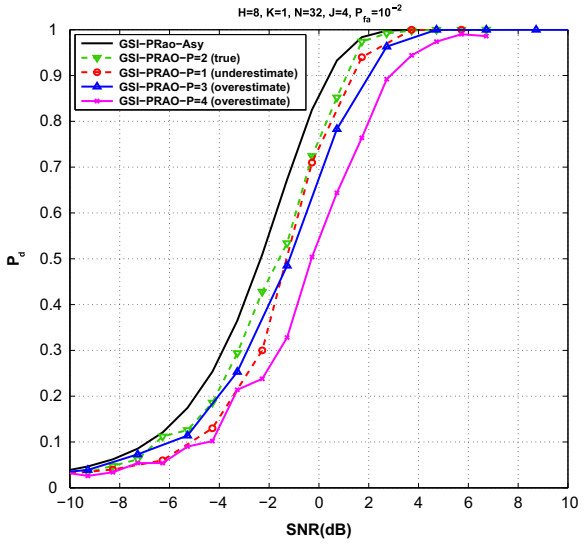

Fig. 6. Probability of detection vs. SNR with AR order mismatch, when $P_f=0.01$, $J=4$, $N=32$, $K=1$ and $\lambda=4$.

4.3. Model mismatched case

The above simulation results are based on two assumptions, i.e., the model order is known, and the disturbance is exactly a multichannel AR process. In this subsection, we evaluate the detection performance of the GSI-PRAO when these assumptions are not met. Firstly, we evaluate the proposed method under the assumption that the disturbance is an AR process but the order is incorrect. Fig. 6 depicts the detection performance of the GSI-PRAO when the model order is underestimated and overestimated, wherein the true AR model order is 2. As it can be seen, the performances of the GSI-PRAO have some but not significant degradation when the model order is underestimated or overestimated. It also shows that the bigger

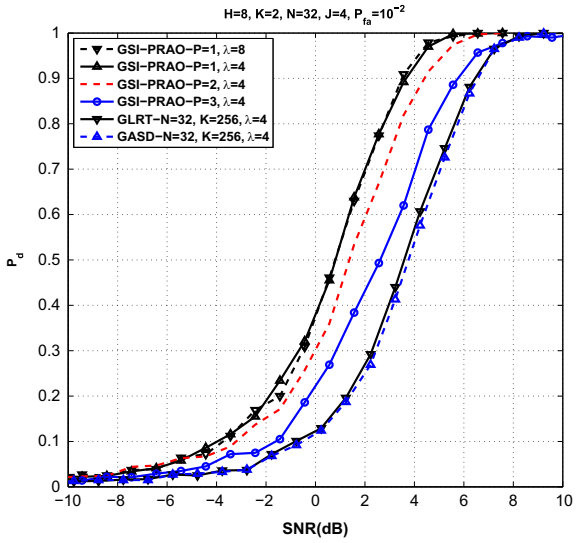

Fig. 7. Probability of detection vs. SNR with disturbance model mismatch, when $P_f=0.01$, $J=4$, $N=32$ and $K=2$.

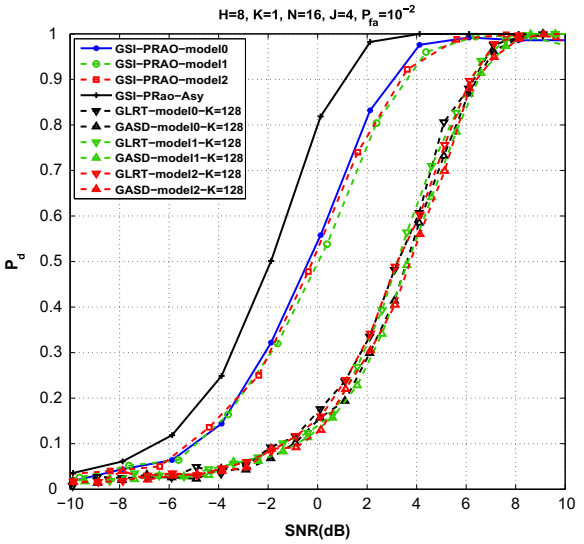

Fig. 8. Probability of detection vs. SNR for different scattering models when $P_f=0.01$, $J=4$, $N=16$, $K=1$ and $\lambda=4$.

the order differs from the true one, the more degradation the GSI-PRAO has. Secondly, we consider that the disturbance is not a precisely AR process. Specifically, we assume that the disturbance is a spatially colored but temporally white Gaussian random vector with the spatial–temporal covariance matrix given by [21]

$$\boldsymbol{R}=\sigma^2\boldsymbol{R}_s\otimes\boldsymbol{I}_t, \tag{42}$$

where $\otimes$ denotes the Kronecker product, σ^2 is the signal to disturbance ratio, the (i,j)th element of $\boldsymbol{R}_s$ is $\rho_s^{|i-j|}$ and $\boldsymbol{I}_t$ is a $N\times N$ identity matrix. In Fig. 7 we compare the GSI-PRAO with the GLRT and GASD assuming that $J=4$, $N=32$, $\rho_s=0.9$, $K=2$ for the GSI-PRAO, $K=256$ for the GLRT and GASD, and two values of λ. It shows that the GSI-PRAO

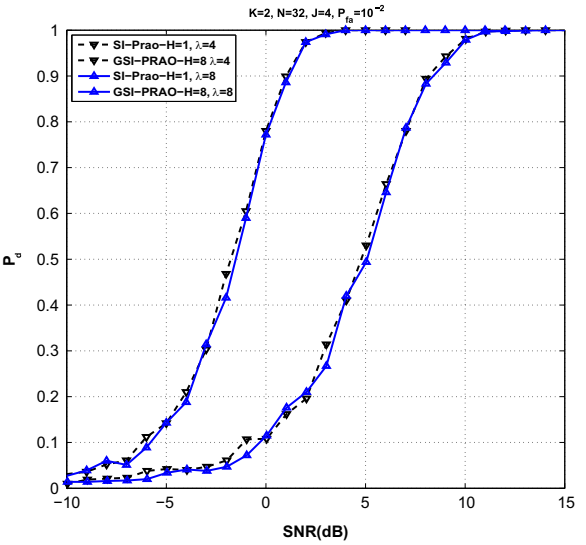

Fig. 9. Probability of detection vs. SNR for PRAO and SI-PRAO when $P_f=0.01$, $J=4$, $N=32$, $K=2$.

performs better when the model order is lower. It is reasonable, since the random process is temporally white, which is suitable for a low AR-model order to approximate the spectrum. However, even when $P=3$ the GSI-PRAO performs better than the GLRT and GASD, which is in accordance with that observed on that AR disturbance model. Interestingly, it also shows that the new receiver still keeps the scaling invariant property.

4.4. MDS models

The aforementioned simulation examples are carried out for detecting a target with uniformly distributed energy, which is Model0 defined in Table 1. In this case, we consider two more different MDS models, termed as Model1 and Model2. Precisely, Model1 represents the case that only one range cell has the strongest scattering energy and the others have uniformly distributed lower scattering energy, while Model2 corresponds to the unresolved point-like target, which is also known to cause the "collapsing loss" due to the presence of cells containing mostly noise [32,9]. Fig. 8 shows that the GSI-PRAO has practically the same detection performance for different MDS models, even for the unresolved point-like target. This result implies that the GSI-PRAO is robust to different MDS models.

In Fig. 9, we compare the GSI-PRAO under model2 with the so-called SI-PRAO introduced in [27], which is the GSI-PRAO for point-like targets, i.e., the GSI-PRAO with $H=1$. The parameters are set as follows: $J=4$, $N=32$, $K=2$, and $H=8$ for the GSI-PRAO. Moreover, we consider two cases of λ, namely $\lambda=4$ and $\lambda=8$. Inspection of the curves highlights that the GSI-PRAO significantly outperforms the SI-PRAO, due to the fact that more noise-only data are available for the GSI-PRAO to estimate the covariance matrix. More precisely, the number of noise-only data for the GSI-PRAO is 9 ($H+K-1=9$), while such number is 2 ($K=2$) for the SI-PRAO.

5. Conclusion

In this paper, we considered the problem of adaptively detecting the range spread target in a partially homogeneous environment. The GSI-PRAO was developed by modelling the disturbance in both test signals and training signals as a multi-channel AR process. The GSI-PRAO was shown to be a sum of each local parametric Rao test of a particular range cell. Each local parametric Rao test used the globe ML estimates of the unknown parameters. The analytical result revealed that the GSI-PRAO was a CFAR test in an asymptotic sense w.r.t. the disturbance covariance and to the unknown power scaling factor. Moreover, in Appendix B we showed the existence and the uniqueness of the ML estimation of the power scaling factor. The simulation results showed that the GSI-PRAO had great performance improvements than the detectors using non-parametric approaches, when the training data was limited. Moreover, the GSI-PRAO have a good robustness to the disturbance model, scaling factor and MDS models.

Acknowledgments

The author would like to give thanks to the handling editor Moeness Amin and anonymous reviewers for their constructional advices and comments. This work was supported by the National Natural Science Foundation of China under Grant No. 61172166.

Appendix A. Derivation of (6)

This appendix is devoted to the derivation of (6). Observe that under H_0 the pdf's of the primary data and the secondary data are

$$f(\boldsymbol{r}_h|\boldsymbol{\theta}) = \left[\frac{1}{\pi^J|\boldsymbol{Q}|}\right]^{H(N-P)} \exp\left\{-\mathrm{tr}\left[\boldsymbol{Q}^{-1}\sum_{h=1}^{H}\sum_{n=P}^{N-1}\boldsymbol{\epsilon}_h(n)\boldsymbol{\epsilon}_h^{\mathrm{H}}(n)\right]\right\}. \tag{A.1}$$

and

$$f(\boldsymbol{r}_k|\boldsymbol{\theta}) = \left[\frac{1}{\pi^J|\lambda\boldsymbol{Q}|}\right]^{K(N-P)} \exp\left\{-\mathrm{tr}\left[\boldsymbol{Q}^{-1}\frac{1}{\lambda}\sum_{k=1}^{K}\sum_{n=P}^{N-1}\boldsymbol{\epsilon}_k(n)\boldsymbol{\epsilon}_k^{\mathrm{H}}(n)\right]\right\}, \tag{A.2}$$

respectively. It follows that their joint pdf is given by

$$f(\boldsymbol{r}|\boldsymbol{\theta}) = \left[\frac{\lambda^{-JK/(K+H)}}{\pi^J|\boldsymbol{Q}|}\right]^{(H+K)(N-P)} \exp\left\{-\mathrm{tr}\left[\boldsymbol{Q}^{-1}\sum_{h=1}^{H}\sum_{n=P}^{N-1}\boldsymbol{\epsilon}_h(n)\boldsymbol{\epsilon}_h^{\mathrm{H}}(n) + \boldsymbol{Q}^{-1}\frac{1}{\lambda}\sum_{k=1}^{K}\sum_{n=P}^{N-1}\boldsymbol{\epsilon}_k(n)\boldsymbol{\epsilon}_k^{\mathrm{H}}(n)\right]\right\}, \tag{A.3}$$

which is equivalent to (6).

Appendix B. ML estimation of λ

In this appendix, we derive the ML estimation of λ, and prove that there is only one $\lambda \in (0, +\infty)$ satisfying (17). The ML estimation derivation is much similar to that in [27].

Put (15) and (16) into (6) and omit the constant parts the log-likelihood function can be written as

$$-\ln f_p(\lambda|\hat{\boldsymbol{A}}, \hat{\boldsymbol{Q}}) \propto \frac{JK}{H+K}\ln\lambda + \ln|T(\lambda)| \tag{B.1}$$

where $|(H+K)(N-P)T(\lambda)| = |(\hat{\boldsymbol{R}}_{rr}(\lambda) - \hat{\boldsymbol{R}}_{tr}^{H}(\lambda)\hat{\boldsymbol{R}}_{tt}^{-1}(\lambda)\hat{\boldsymbol{R}}_{tr}(\lambda))|$ and $\propto$ means "proportional to". Using (18), (19) and (14) $|(H+K)(N-P)T(\lambda)|$ can be denoted as

$$|(H+K)(N-P)T(\lambda)| = \frac{|\hat{\boldsymbol{R}}_H + \frac{1}{\lambda}\hat{\boldsymbol{R}}_K|}{|\hat{\boldsymbol{R}}_{tt}(\lambda)|} \tag{B.2}$$

since

$$\frac{|\hat{\boldsymbol{R}}_H + \frac{1}{\lambda}\hat{\boldsymbol{R}}_K|}{|\hat{\boldsymbol{R}}_{tt}(\lambda)|} = |(\hat{\boldsymbol{R}}_{rr}(\lambda) - \hat{\boldsymbol{R}}_{tr}^{H}(\lambda)\hat{\boldsymbol{R}}_{tt}^{-1}(\lambda)\hat{\boldsymbol{R}}_{tr}(\lambda))| \tag{B.3}$$

Consequently, we have

$$-\ln f_p(\lambda|\hat{\boldsymbol{A}}, \hat{\boldsymbol{Q}}) \propto \frac{JK}{H+K}\ln\lambda + \ln\left|\hat{\boldsymbol{R}}_H + \frac{1}{\lambda}\hat{\boldsymbol{R}}_K\right| - \ln|\hat{\boldsymbol{R}}_{tt}(\lambda)| \tag{B.4}$$

on the other hand, the log-likelihood function of the non-parametric method can be written as

$$\ln f_{np}(\lambda|\hat{\boldsymbol{R}}) = \ln[e^{-JN}\pi^{-JN}\lambda^{-JNK/(H+K)}|\boldsymbol{S}(\lambda)|]^{(H+K)} \propto -\left(\frac{JNK}{H+K}\ln\lambda + \ln|\boldsymbol{S}(\lambda)|\right) \tag{B.5}$$

where the ML estimation of time–space covariance matrix $\boldsymbol{R}$ is $\boldsymbol{S}(\lambda)$. Particularly it is

$$(H+K)\boldsymbol{S}(\lambda) = \sum_{h=1}^{H}\boldsymbol{r}_h\boldsymbol{r}_h^H + \frac{1}{\lambda}\sum_{k=1}^{K}\boldsymbol{r}_k\boldsymbol{r}_k^H \tag{B.6}$$

Let $\boldsymbol{E} = \sum_{h=1}^{H}\boldsymbol{r}_h\boldsymbol{r}_h^H$ and $\boldsymbol{F} = \sum_{k=1}^{K}\boldsymbol{r}_k\boldsymbol{r}_k^H$, and take the derivatives of (B4) and (B5) w.r.t. λ and equate them to zero, we have (17) and (B.7), respectively

$$\frac{JNK}{H+K} - \sum_{i=1}^{JN}\frac{1}{1+\lambda s_i} = 0 \tag{B.7}$$

where $s_i \geq 0$ is the eigenvalue of $\boldsymbol{F}^{-1/2}\boldsymbol{E}\boldsymbol{F}^{-1/2}$, since $\boldsymbol{E}$ and $\boldsymbol{F}$ are both positive semi-definite, and we use the fact that

$$\frac{\partial}{\partial\lambda}\ln\left|\boldsymbol{B} + \frac{1}{\lambda}\boldsymbol{C}\right| = \sum_{i=1}^{M}\frac{-1}{\lambda(1+\lambda b_i)} \tag{B.8}$$

where $b_i \geq 0$ is the eigenvalue of $\boldsymbol{C}^{-1/2}\boldsymbol{B}\boldsymbol{C}^{-1/2}$. Define

$$g(\lambda) = \frac{JK}{H+K} - \sum_{i=1}^{J(P+1)}\frac{1}{1+\lambda\tau_i} + \sum_{i=1}^{JP}\frac{1}{1+\lambda\gamma_i} \tag{B.9}$$

$$h(\lambda) = \frac{JNK}{H+K} - \sum_{i=1}^{JN}\frac{1}{1+\lambda s_i} \tag{B.10}$$

Note that $g(\lambda)$ and $h(\lambda)$ are both continuous functions on $(0, +\infty)$, and observe that

$$\lim_{\lambda\to 0} g(\lambda) = \frac{JK}{H+K} - J < 0 \tag{B.11}$$

$$\lim_{\lambda\to 0} h(\lambda) = \frac{JNK}{H+K} - JN < 0 \tag{B.12}$$

$$\lim_{\lambda\to \infty} g(\lambda) = \frac{JK}{H+K} > 0 \tag{B.13}$$

$$\lim_{\lambda\to \infty} h(\lambda) = \frac{JNK}{H+K} > 0 \tag{B.14}$$

which implies that there is at least one $\lambda \in (0, +\infty)$ giving $g(\lambda) = 0$ or $h(\lambda) = 0$. As we mentioned in the end of Section 2 that the λ in $CN(0, \lambda \boldsymbol{R})$ and the λ in $CN(0, \lambda \boldsymbol{Q})$ are exactly the same. So if there is only one $\lambda \in (0, +\infty)$ for $h(\lambda) = 0$, there is only one $\lambda \in (0, +\infty)$ for $g(\lambda) = 0$. The first-order derivative of $h(\lambda)$ w.r.t. λ is

$$\frac{\partial}{\partial \lambda} h(\lambda) = \sum_{i=1}^{JN} \frac{b_i}{(1+\lambda b_i)^2} > 0 \tag{B.15}$$

So $h(\lambda)$ is a monotonically increasing function with $\lim_{\lambda\to 0} h(\lambda) < 0$ and $\lim_{\lambda\to\infty} h(\lambda) > 0$. This implies that λ is unique in $(0, +\infty)$ for $h(\lambda) = 0$. Moreover, if $\exists \lambda_1 \neq \lambda$ satisfying $g(\lambda_1) = 0$, such that $h(\lambda_1) = 0$, since λ is the unique solution for $h(\lambda) = 0$, we have $\lambda_1 = \lambda$, that is contrary to the assumption. So λ is the unique solution for $g(\lambda) = 0$, hence λ is unique in $(0, +\infty)$.

References

[1] E.J. Kelly, An adaptive detection algorithm, IEEE Trans. Aerosp. Electron. Syst. 22 (March (1)) (1986) 115–127.

[2] F.C. Robey, D.L. Fuhrmann, E.J. Kelly, R. Nitzberg, A CFAR adaptive matched filter detector, IEEE Trans. Aerosp. Electron. Syst. 29 (March (1)) (1992) 208–216.

[3] A. De Maio, A new derivation of the adaptive matched filter, IEEE Signal Process. Lett. 11 (2004) 792–793.

[4] A. De Maio, Rao test for adaptive detection in gaussian interference with unknown covariance matrix, IEEE Trans. Signal Process. 55 (2007) 3577–3584.

[5] D. Orlando, G. Ricci, Adaptive radar detection and localization of a point-like target, IEEE Trans. Signal Process. 59 (September (9)) (2011) 4086–4096.

[6] D. Orlando, G. Ricci, A Rao test with enhanced selectivity properties in homogeneous scenarios, IEEE Trans. Signal Process. 58 (October (10)) (2010) 5385–5390.

[7] W. Liu, W. Xie, J. Liu, Y. Wang, Adaptive double subspace signal detection in Gaussian background-part I: homogeneous environments, IEEE Trans. Signal Process. 62 (September (9)) (2014) 2345–2357.

[8] W. Liu, W. Xie, Y. Wang, A Wald test with enhanced selectivity properties in homogeneous environments, EURASIP J. Adv. Signal Process. 2013 (14) (2013).

[9] E. Conte, A. De Maio, G. Ricci, GLRT-based adaptive detection algorithms for range-spread targets, IEEE Trans. Signal Process. 49 (July (7)) (2001) 1336–1348.

[10] F. Bandiera, D. Orlando, G. Ricci, CFAR detection of extended and multiple point-like targets without assignment of secondary data, IEEE Signal Process. Lett. 13 (April (4)) (2006) 240–243.

[11] F. Bandiera, O. Besson, D. Orlando, G. Ricci, L.L. Scharf, GLRT-based direction detectors in homogeneous noise and subspace interference, IEEE Trans. Signal Process. 55 (June (6)) (2007) 2386–2394.

[12] F. Bandiera, A. De Maio, A. Greco, G. Ricci, Adaptive radar detection of distributed targets in homogeneous and partially homogeneous noise plus subspace interference, IEEE Trans. Signal Process. 55 (April (4)) (2007) 1223–1237.

[13] F. Bandiera, D. Orlando, G. Ricci, CFAR detection strategies for distributed targets under conic constraints, IEEE Trans. Signal Process. 57 (September (9)) (2009) 3305–3316.

[14] C. Hao, J. Yang, X. Ma, C. Hou, D. Orlando, Adaptive detection of distributed targets with orthogonal rejection, IET Radar Sonar Navigat. 6 (July (6)) (2012) 483–493.

[15] C. Hao, F. Bandiera, J. Yang, D. Orlando, S. Yan, C. Hou, Adaptive detection of multiple point-like targets under conic constraints, Prog. Electromag. Res. 129 (2012) 231–250.

[16] A. De Maio, A. Farina, K. Gerlach, Adaptive detection of range spread targets with orthogonal rejection, IEEE Trans. Aerosp. Electron. Syst. 43 (April (2)) (2007) 738–752.

[17] A. Aubry, A. De Maio, L. Pallotta, A. Farina, Radar detection of distributed targets in homogeneous interference whose inverse covariance structure is defined via unitary invariant functions, IEEE Trans. Signal Process. 61 (October (20)) (2013) 4949–4961.

[18] P.K. Hughes II, A high resolution radar detection strategy, IEEE Trans. Aerosp. Electron. Syst. AES-19 (September) (1983) 663–667.

[19] J.R. Roman, M. Rangaswamy, D.W. Davis, Q. Zhang, B. Himed, J.H. Michels, Parametric adaptive matched filter for airborne radar applications, IEEE Trans. Aerosp. Electron. Syst. 36 (April (2)) (2000) 677–692.

[20] J. Li, G. Liu, N. Jiang, P. Stoica, Moving target feature extraction for airborne high-range resolution phased-array radar, IEEE Trans. Signal Process. 49 (February) (2001) 277–289.

[21] Y. Jiang, P. Stoica, J. Li, Array signal processing in the known waveform and steering vector case, IEEE Trans. Signal Process. 52 (January) (2004) 23–25.

[22] H. Li, K.J. Sohn, B. Himed, The PAMF detector is a parametric Rao test, in: Proceedings of the 39th Asilomar Conference on Signals, Systems and Computers, Pacific Grove, CA, November 2005.

[23] K.J. Sohn, H. Li, B. Himed, Parametric Rao test for multichannel adaptive signal detection, IEEE Trans. Aerosp. Electron. Syst. 43 (July) (2007) 920–933.

[24] K.J. Sohn, H. Li, B. Himed, Parametric GLRT for multichannel adaptive signal detection, IEEE Trans. Signal Process. 55 (November) (2007) 5351–5360.

[25] P. Wang, H. Li, B. Himed, A new parametric GLRT for multichannel adaptive signal detection, IEEE Trans. Signal Process. 58 (1) (2010) 317–325.

[26] P. Wang, H. Li, B. Himed, Generalised parametric Rao test for multichannel adaptive detection of range-spread targets, IET Signal Process. 6 (July (5)) (2012) 404–412.

[27] P. Wang, H. Li, B. Himed, Parametric Rao tests for multichannel adaptive detection in partially homogeneous environment, IEEE Trans. Aerosp. Electron. Syst. 47 (2011) 1850–1862.

[28] C. Hao, X. Ma, X. Shang, Adaptive detection of distributed targets in partially homogeneous environment with Rao and Wald tests, Signal Process. 92 (April (4)) (2012) 926–930.

[29] S.M. Kay, Fundamentals of Statistical Signal Processing: Detection Theory, vol. II, Prentice-Hall, Englewood Cliffs, NJ, 1998.

[30] Jaime R. Roman, Dennis W. Davis, Multichannel System Identification and detection using output data techniques, Technical Report RL-TR-97-5, vol. I, Air Force Research Lab, Rome Site, 1997.

[31] James H. Michels, Pramod K. Varshney, Donald D. Weiner, Synthesis of correlated multichannel random processes, IEEE Trans. Signal Process. 42 (February (2)) (1994).

[32] R. Nitzberg, Effect of a few dominant specular reflectors target model upon target detection, IEEE Trans. Aerop. Electron. Syst. AES-14 (July) (1978) 198–200.